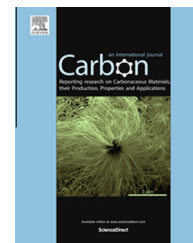


Available at www.sciencedirect.com

ScienceDirect

journal homepage: www.elsevier.com/locate/carbon

Quantitative nanomechanical characterization of the van der Waals interfaces between carbon nanotubes and epoxy



Xiaoming Chen^a, Liuyang Zhang^b, Meng Zheng^a, Cheol Park^{c,d}, Xianqiao Wang^{b,*}, Changhong Ke^{a,*}

^a Department of Mechanical Engineering, State University of New York at Binghamton, Binghamton, NY 13902, USA

^b College of Engineering, University of Georgia, Athens, GA 30602, USA

^c NASA Langley Research Center, Hampton, VA 23681, USA

^d Department of Mechanical and Aerospace Engineering, University of Virginia, Charlottesville, VA 22904, USA

ARTICLE INFO

Article history:

Received 15 August 2014

Accepted 21 October 2014

Available online 27 October 2014

ABSTRACT

Interfacial interactions between carbon nanotubes (CNTs) and polymer matrices play a critical role in the bulk mechanical performance of CNT-reinforced polymer nanocomposites, but their mechanisms remain elusive after over a decade of research. Here we present an *in situ* electron microscopy nanomechanical study of the non-covalent van der Waals interfaces between individual CNTs and epoxy resins in conjunction with atomistic simulations. By pulling out individual double-walled CNTs from Epon 828 films inside a high resolution electron microscope, the nanomechanical measurements capture the shear lag effect on CNT–epoxy interfaces. The maximum pull-out load of CNT–epoxy interfaces is found to be about 44% higher than the recently reported value for CNT–poly(methyl methacrylate) (PMMA) interfaces that were characterized using the same experimental technique and the same batch of dispersed CNTs. The higher interfacial strength of CNT–epoxy interfaces is partially attributed to the forced molecular deformations of aromatic rings in epoxy chains in the vicinity of the binding interface, which is supported by molecular dynamics simulations of the CNT–polymer interfacial interactions. The research findings contribute to a better understanding of the local load transfer on the tube–polymer interface and the tube’s reinforcing mechanism, and ultimately the optimal design and performance of nanotube-reinforced polymer nanocomposites.

© 2014 Elsevier Ltd. All rights reserved.

1. Introduction

The quest for light-weight and high-strength materials is of importance for the aerospace industry as a result of an increasingly demanding payload projected for next-generation flying vehicles. Carbon nanotubes (CNTs), a type of

ultra-strong, resilient and tubular nanostructure, have been holding great promise for disruptive fiber-reinforced polymer nanocomposites technologies [1,2] since their discovery [3]. Although substantial advances have been achieved over the past two decades, the bulk mechanical properties of CNT-reinforced polymer nanocomposites remain unsatisfactory

* Corresponding authors.

E-mail addresses: xqwang@uga.edu (X. Wang), cke@binghamton.edu (C. Ke).

<http://dx.doi.org/10.1016/j.carbon.2014.10.065>

0008-6223/© 2014 Elsevier Ltd. All rights reserved.

and far from their anticipated levels. Among all the technical challenges, lack of understanding of nanotube–polymer interfaces is considered to be a vital, but insurmountable issue in realizing the reinforcing effect of these nano-fillers. This is because the realization of the reinforcing effect of the high-strength additive nanotubes relies on an adequate load transfer on the tube–polymer interface. However, the prevalent failure mode for nanotube-reinforced polymer nanocomposites occurs on the interface, shown as the pull-out of tubes from polymer matrices. The nanotube–polymer interface involves sophisticated physical–chemical adsorption phenomenon. In particular, prior studies on the polymerization dynamics in the presence of CNTs [4–6] suggest that nanotube additives are much more than passive contributors to the mechanical enhancement of polymers. It is quite likely that these nanotubes not only mix into the polymer, but also initiate and participate in reactions that lead to microstructural development of polymer in the neighborhood of nanotubes [7–10]. A recent study reports that the polymer chains close to the binding interface with CNTs have more compact packing, higher orientation, and better mechanical properties compared with bulk polymers [11].

Direct quantitative measurements of the interfacial strength of individual nanotubes with polymers are essential to a complete understanding of the interfacial stress transfer and their reinforcing mechanisms. However, a vast majority of the reported studies on CNT-reinforced polymers in the literature was carried out at a macroscopic level, and can at most be used to evaluate interfacial strength properties qualitatively and indirectly [12,13]. Reports on direct, quantitative, and microscopic measurements of the interfaces formed by individual nanotubes or nanofibers with polymers remain quite limited [14–22]. It is noted that epoxy is the most popular polymer employed in the reported single-tube measurements [14], which is most probably due to the wide usage of epoxy resin in practical applications. Notably, Wagner and his co-workers [23] reported the first single-tube pull-out event by stretching a multi-walled CNT (MWCNT) out of an epoxy film inside a transmission electron microscope (TEM). Subsequently, they reported quantitative measurements inside atomic force microscopes (AFM) [17–20]. Recently, single-tube pull-out measurements based on microelectromechanical system (MEMS)-based loading cells on the interfaces of CNT–epoxy and carbon nanofiber (CNF)–epoxy were reported by Lou et al. [21,22] and Chasiotis et al. [14], respectively. The key results from these studies are summarized in Table 1. In spite of all these valuable advances, several limitations and challenges remain yet to be solved. *First*, systematic studies of the nanotube–polymer interface require measurements cross a wide range of the embedded tube lengths. This is of particular importance to capture the shear lag effect [20,24] on the local stress transfer on the interface. By considering the nanotube pull-out as a crack initiation and propagation process, shear lag effect indicates that effective load transfer occurs only within a certain embedded length. However, some of the reported studies are based on quite limited data points ($n < 5$), from which accurate and reliable knowledge on the interfacial strength cannot be established. *Second*, experimental data on interfaces between tubes of small

numbers of walls and diameters and polymers remain extremely scarce. In nanotube-reinforced polymer nanocomposites, the stress in the polymer is transferred to the outermost shell of the tube through the tube–polymer interface, while the inner tube shells contribute little to load bearing due to the weak inter-layer van der Waals (vdW) interaction. In other words, only the outermost shell of the tube contributes to its reinforcing effect. Therefore, it is of advantage to use small-diameter tubes in exploring their polymer nanocomposites. However, the reported studies as listed in Table 1 are based on multi-walled CNTs or single-walled CNT (SWCNT) bundles of quite large diameters, and the interface formed by tubes of sub-10 nm in outer diameter and polymers remains largely unexplored. *Third*, it is challenging to draw solid conclusions through comparison of the reported data with large scattering. This is because the data were obtained using different single-tube measurement techniques and based on different types of nanotubes and/or polymers. The tube–polymer interfacial interaction depends on the types of tubes and polymers. The molecular structure of polymer matrices, in particular the monomer structures such as aromatic rings, has a substantial influence on its binding affinity with CNTs. The knowledge of the interfacial strength helps to understand and elucidate the role of these molecular structures and their atomistic-level reactions to the binding surface of CNTs. To the best of our knowledge, experimental studies on interfaces that are formed by the same type of tubes with different types of polymers and characterized using the same single-tube measurement technique remain unexplored. The lack of such critical data makes it an intractable task to evaluate and compare the interfaces based on different types of polymer matrices. Recently, our research group proposed an *in situ* electron microscopy nanomechanical single-tube testing scheme [24], which is promising to overcome the above-mentioned limitations and challenges. Our nanomechanical scheme was successfully demonstrated by testing the interface formed by double-walled CNTs (DWCNTs) and poly(methyl methacrylate) (PMMA). Our single-tube pull-out approach is based on a novel preparation method of the tube–polymer interface that is formed inside a sandwiched polymer/tube/polymer thin-film composite. Our proposed testing scheme is envisioned to be capable of quantifying the strength of interfaces formed by a wide variety of polymers (e.g., both thermoplastic and thermoset) and nanostructures with a broad range of diameters (i.e., from a few to hundreds of nanometers) [24].

In this paper, we present a nanomechanical study of the interfacial strength between individual CNTs and epoxy using our *in situ* electron microscopy single-tube pull-out testing techniques. Our results report, *for the first time*, that the maximum pull-out load of CNT–epoxy interfaces is about 44% higher than that of CNT–PMMA interfaces. The observed high interfacial strength of CNT–epoxy interfaces is analyzed from the perspectives of the chemical compositions and molecular structures of epoxy, and is ascribed partially to the translation and rotation of the aromatic rings in epoxy resins. Our analysis is supported by the results from the molecular dynamics (MD) simulations of the relaxation of the model epoxy and PMMA chains on

Table 1 – Comparison of the calculated interfacial fracture energy and shear strength of the CNT-epoxy interface based on our *in-situ* single-tube pull-out measurements with those experimental and molecular dynamics (MD) simulation data reported in the literature.

Type of CNT/CNF (diameter in nm)	Epoxy matrix	Interfacial fracture energy (J/m^2)	Average shear strength (MPa)	Maximum shear strength (MPa)	Reference
DWCNT (3.1 ± 1)	Epon 828	1.07–1.5	202 ± 52	628 ± 29	Present study
		0.29–0.40	130 ± 34	270 ± 12	
		0.116–0.162	96 ± 25	151 ± 7	
MWCNT (8.2–24)	Araldite LY 564	0.9–36.9	35–376	–	Wagner et al. [17]
SWNT rope (11.6)	Araldite LY 564	25.6	366 ± 74	–	Wagner et al. [17]
MWCNT (80 ± 30)	Epoxy	–	30 ± 7	–	Wagner et al. [20]
MWCNT (75 ± 20)	Epon 828	0.05–0.25	6.24 ± 3.6	–	Lou et al. [21]
SWCNT (0.78)	Epon 862	–	170 (MD)	–	Liu et al. [25]
SWCNT (1.33)	SU-8	–	138 (MD)	–	Wong et al. [26]
SWCNT (1.36)	Epon 862	–	75 (MD)	–	Gou et al. [27]
CNF (240–480)	Epikote 862	–	169–632	–	Haque et al. [15]
CNF (450–2000)	Epon 828	1.9 ± 0.9	106 ± 29	224 ± 60	Chasiotis et al. [14]

the surface of CNTs. This study demonstrates that our *in situ* nanomechanical single-tube pull-out experimental technique can be used to characterize the unique nanomechanical signatures of the interfaces formed by CNTs with a variety of polymer matrices, thus enabling a convincing quantification and comparison of the interfacial strength across different nanotube-polymer nanocomposite systems. The research findings presented in this paper contribute to a better understanding of the load transfer on the tube-polymer interface and the tube's reinforcing mechanism, and ultimately the optimal design and performance of nanotube-reinforced polymer nanocomposites.

2. Experimental

2.1. Sample preparation

The preparation of all the samples employed in this study mostly follows the same protocols reported in Ref. [24]. Double-walled CNTs employed in this study were dispersed in deionized (DI) water using ultrasonication with the aid of ionic surfactants sodium dodecylbenzenesulfonate (NaDBS). The dispersed nanotubes were characterized inside a high resolution AFM (XE-70, Park systems). Their lengths are found to be mostly less than 2 μm , and their outer diameters are normally distributed and are mostly within 2.0–4.2 nm (>92%). The surface chemistry of the dispersed nanotubes was characterized by Fourier transform infrared spectroscopy (FTIR) using a Nicolet 8700 FTIR Spectrometer from Thermo Electron Corp.

The employed Epon 828 difunctional bisphenol A/epichlorohydrin epoxy resin compounded and curing agent EPIKURE 3200 aminoethyl piperazine (AEP) were purchased from Momentive Specialty Chemicals Inc. The CNT-epoxy interfaces employed in the single-tube nanomechanical pull-out tests were prepared inside sandwiched polymer/tube/polymer thin-film composites. In brief, Epon 828 with curing agent at a weight ratio of 5:1 was dissolved in toluene at a weight ratio of 1:1. The solution was then spin-coated on a clean silicon wafer to form a thin epoxy resin layer ($\sim 1 \mu\text{m}$ in thickness after curing), followed by the deposition of a well-dispersed double-walled CNTs solution and another polymer layer. The sandwich-like CNT-embedded thin-film polymer was cured at 25 $^\circ\text{C}$ for 12 h and 150 $^\circ\text{C}$ for an additional two hours in a vacuum oven. The thin-film composite was broken by means of cracking the substrate using a diamond scribe, and some of the embedded tubes were exposed as straight free-standing cantilever structures. It is noted that the deposited CNTs on the polymer surface were rinsed with DI water before the deposition of the top polymer layer to remove possible surfactant residues, which may have a substantial influence on the tube-polymer interfacial interactions [28,29]. The tubular structures of CNTs prepared using this method were inspected using high resolution transmission electron microscopy (HRTEM) techniques (a representative HRTEM image is shown as Fig. S1 in the Supplementary Materials). The HRTEM inspection confirms that CNTs have clean structural surfaces. The effect of the surfactant residue on the tube-polymer interface is considered to be quite minimal.

2.2. Single-tube pull out measurements

The *in-situ* pull-out tests were performed inside an FEI Nano-lab 600 electron microscope. Silicon AFM probes (model CSG 01, NT-MDT) were employed as the force sensors employed in the pull-out tests. The spring constant of each employed AFM probe was calibrated using a thermal tuning method and was found to be within the range of 0.04–0.09 N/m. The pull-out load is calculated based on the spring constant of the AFM force sensor and its last recorded deflection in the pull-out test with a resolution of about 0.5–1 nN. The AFM sensor was mounted to a 3D piezo stage that possesses 1 nm displace resolution in the X–Y–Z axes and was controlled to move at a rate of approximately 0.5–1 $\mu\text{m/s}$. The embedded tube length is measured directly using the high resolution electron beam with a resolution of a few nanometers.

2.3. Molecular dynamics simulations

MD simulations are carried out by using OPLS-AA force field [30]. The OPLS-AA force field has been widely used in molecular analysis of polymer materials. The functional form of the OPLS-AA force field is evaluated as the sum of four individual energy contributions that are associated with bond stretching, angle bending, torsion and non-bonded part, respectively. The non-bonded energy contribution is computed as a sum of Coulomb and 12-6 Lennard-Jones contributions for pairwise intra- and intermolecular interactions related to electrostatic and van der Waals interactions. All the parameters used in the energy calculation are taken directly from the standard OPLS-AA. Energy minimization is performed to find the thermally stable configuration and achieve a conformation with minimum potential energy for the system. After the equilibrium state is achieved, NVT ensemble simulations with temperature 300 K are carried out based on the Berendsen thermostat [31]. The velocity Verlet time stepping method is utilized with an integration time step of 0.5 fs. A cutoff distance of 10 Å is used for all potentials. To speed up computation, the atoms in DWCNTs are fixed to their initial positions, which facilitates the characterization of the polymer conformation with respect to the DWCNT.

3. Results and discussion

3.1. In situ electron microscopy single-tube nanomechanical pull-out measurements

The interfacial binding strength of individual CNTs with epoxy was first characterized using our *in situ* electron microscopy single-tube nanomechanical pull-out techniques. Fig. 1(a)–(c) schematically shows the key steps in the single-tube nanomechanical pull-out measurements inside a high resolution scanning electron microscope (SEM). In this testing scheme, the CNT–polymer interface is prepared using a polymer/nanotube/polymer sandwich scheme. The tip of an AFM force sensor that is mounted to a 3D piezo stage is first controlled to approach the free end of a nanotube that is partially embedded into a thin-film polymer, as illustrated in Fig. 1(a).

Subsequently, the free end of the tube is spot-welded to the tip of the AFM sensor by means of electron-beam-induced deposition (EBID) of platinum (Pt) [32] (Fig. 1(b)). It is noted that the deposited Pt using this approach will not only coat the window area specified during the spot deposition process, but also cover the whole extruding portion of the tube (typically 100–500 nm in length) through diffusion [33]. Then, the AFM force sensor is displaced incrementally to apply an increasing tensile stretching force until the embedded portion of the tube is fully pulled out of the polymer film (Fig. 1(c)). It is noted that the coverage of the Pt on the extruding portion of the tube helps the measurement of the tube embedded length, while not tampering with the CNT–polymer interface and its interfacial strength.

The preparation of desirable pull-out samples is of importance not only to the success of the pull-out test, but also to the next-stage interpretation and analysis of the experimental data. For instance, to ensure that the tube is pulled out from the polymer in a pure stretching mode, both the extruding and the embedded portions of the chosen tube need to be straight, and its orientation is aligned with the stretching force direction. The tube used in our pull-out tests are DWCNTs, whose outer diameters are found, by AFM imaging, to be normally distributed and mostly within 2.0–4.2 nm (>92%). The lengths of the dispersed tubes are found to be mostly less than 2 μm . Our AFM imaging measurements show that the employed dispersed tubes are able to stay straight on the polymer surface after spin-coating deposition. Surface chemistry of the employed tubes is another important factor in the understanding of the CNT–polymer interface. The surface chemistry of the dispersed nanotubes was characterized by using Fourier transform infrared spectroscopy (FTIR) and found to be free of functional groups such as C=O, CH and OH [24]. Therefore, the interfacial interaction between CNTs, which exhibit an even charge distribution [34], and polymers that were characterized in our single-tube pull-out tests are based on non-covalent vdW interactions. Epon 828 is selected as the epoxy resin in this study because it is widely used in various industries and was also employed in two recent single-tube pull-out measurements [14,21]. Fig. 1(d)–(f) shows three selected SEM snapshots of a represented single-tube measurement of CNT–epoxy interfaces, which correspond to Fig. 1(a)–(c), respectively. The pull-out load was measured to be 206 nN. After the pull-out test, the embedded tube length in the epoxy film was measured to be 416 nm from the zoom-in view SEM image shown in Fig. 1(f). In our pull-out tests, it is noted that a high resolution electron beam was employed to monitor the nanomanipulation processes, the mechanical response of the tested tube, and the displacement and deflection of the AFM force sensor. While the electron beam irradiation reportedly has a material influence on the strength of nanotubes [35], it is expected to have little-to-no effect on the nanotube–polymer interfacial strength. This is because the nanotube–polymer interface was buried below a layer of polymer of $\sim 1 \mu\text{m}$ in thickness and not exposed directly to the electron beam.

It can be clearly seen from Fig. 1(f) that the whole tube, including the embedded segment, remained straight after pull-out and was aligned nearly parallel to the stretching direction. This is a strong indication that the embedded tube

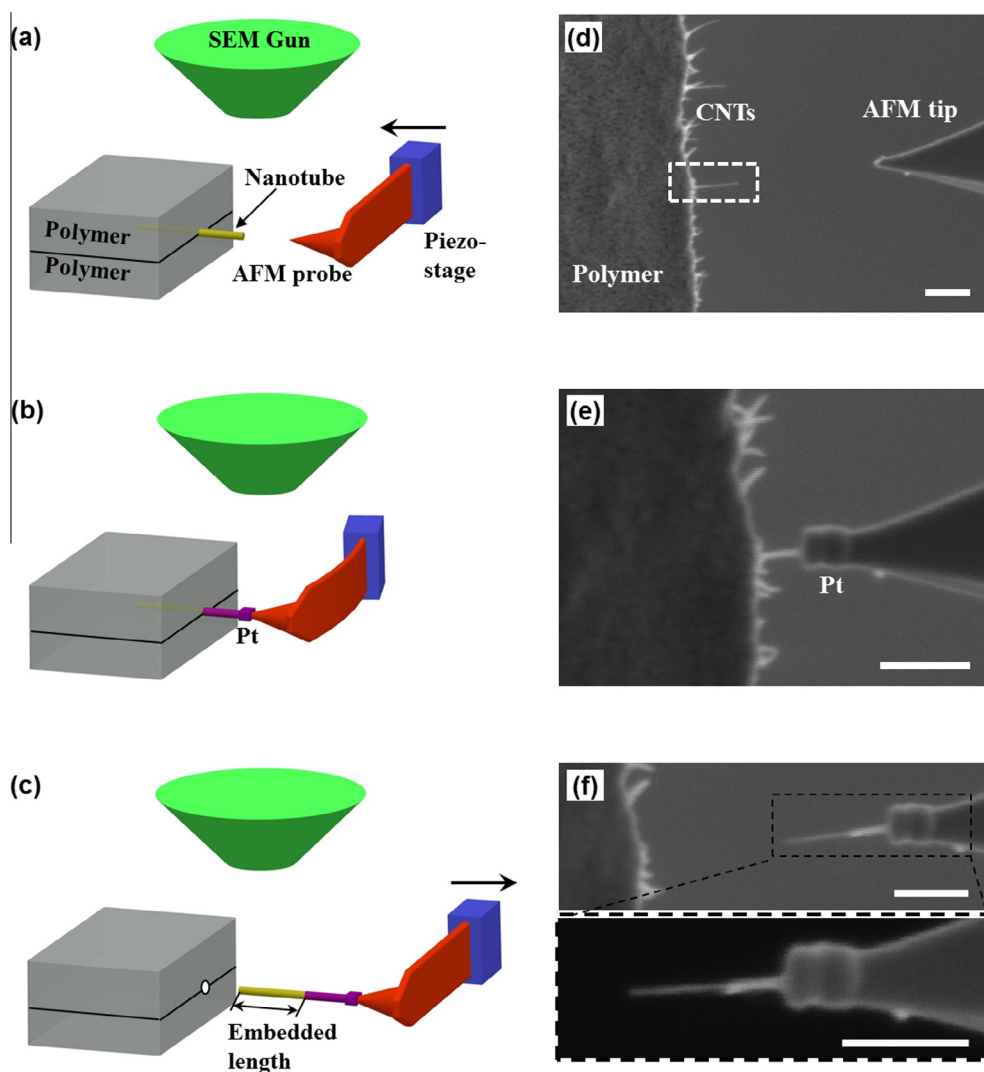


Fig. 1 – 3D Illustration of our *in situ* SEM nanomechanical single-tube pull-out scheme and selected results of one representative pull-out measurement: (a) The tip of an AFM force sensor is controlled to approach the free end of a selected protruding nanotube; (b) The nanotube free end is welded to the AFM tip using EBID of Pt; (c) The tube is pulled out completely from the polymer. (d)–(f) Three selected SEM snapshots of one representative single-tube pull-out test, corresponding to the schematic drawings shown in (a)–(c), respectively. The bottom image in (f) is a zoom-in view of the pulled-out nanotube. All scale bars represent 500 nm. (A colour version of this figure can be viewed online.)

in the polymer was straight and also aligned to the pulling force direction. To further confirm that the orientations of the tested tube before and after the pull-out measurement remain intact, we performed control tests as illustrated in Fig. 2(a), in which the chosen tube was originally oriented in a substantial angle to the pulling force direction. After the pull-out test, the whole tube is expected to stay straight and remain in the same orientation as its initial protruding segment. The snapshots in Fig. 2(b) show one of the actual pull-out tests. The initial orientation angle of the free-standing portion of the tube with respect to the pulling force direction or the axis of the AFM probe tip is measured to be 40° . After being pulled out of the polymer, the whole tube remained straight with an orientation angle of 44° , as shown in the inset snapshot in Fig. 2(b). Our results clearly show that there is little alternation to the nanotube orientation during the pull-out process, which can be ascribed to the firm fixed

clamping of the tube's free end to the AFM tip. The control test shown in Fig. 2(b) directly supports our statement that the orientation of the tube remains largely intact after the pull-out test in our single-tube pull-out testing scheme. Therefore, the measured pull-out load for the test shown in Fig. 1(d)–(f) equals the maximum bearable load on the tube–polymer interface. However, we must point out that the tube undergoes not only stretching, but also bending deformations when its initial orientation does not align with the pulling force direction. In such case, the analysis of the nanotube–polymer interfacial strength must take into account the bending effect, which is beyond the scope of this paper. Data recorded in such pull-out measurements are excluded in the data analysis presented in the next section.

It is noted that the pull-out test as illustrated in Fig. 1(a)–(c) may not always yield a successful pull-out as the one shown in Fig. 1(f). The following two scenarios of the outcome of our

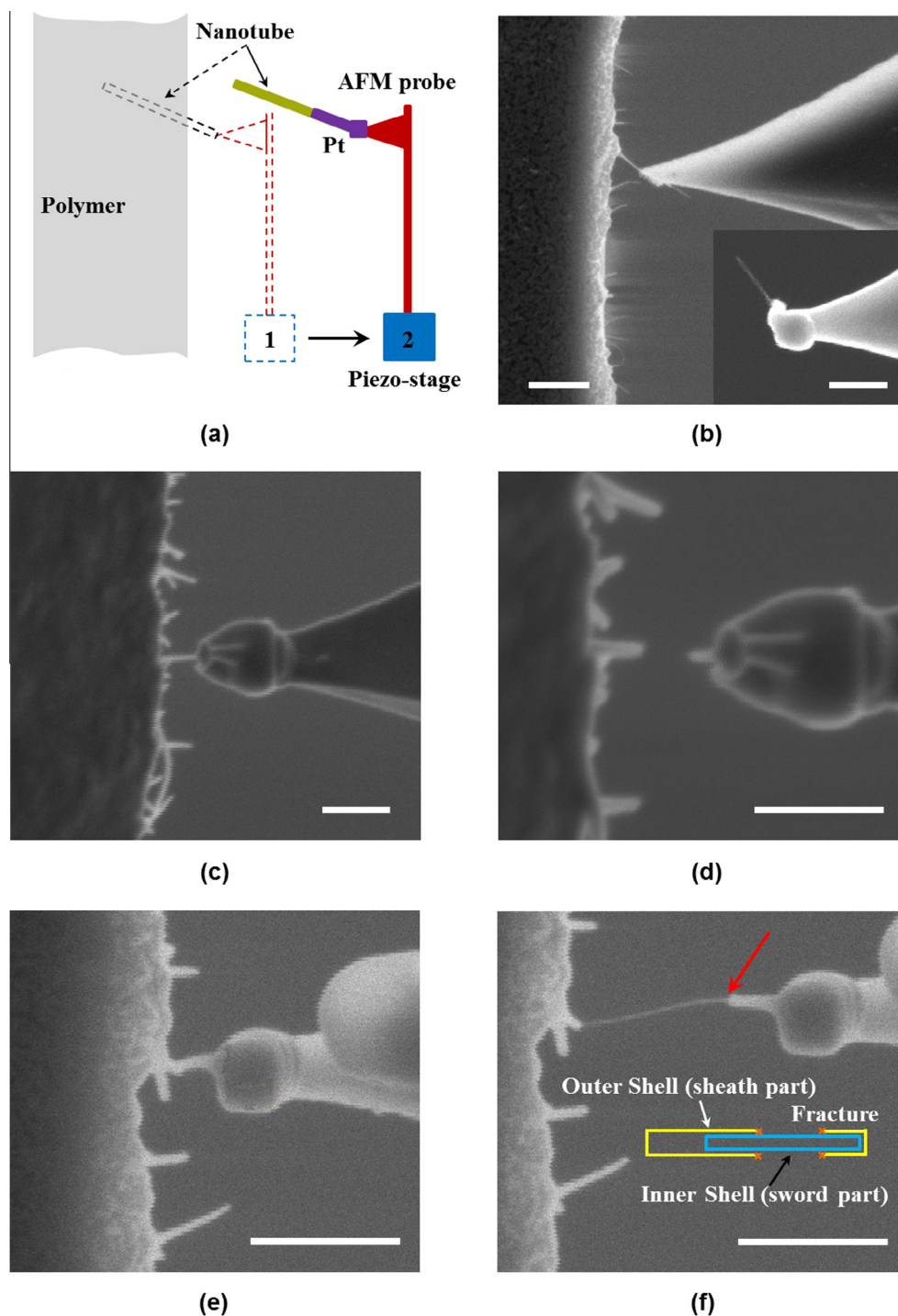


Fig. 2 – Three scenarios observed in our *in situ* SEM nanomechanical single-tube pull-out tests. (i) Pulling out a tube of an initial angle to the pulling force direction: (a) schematic drawing; (b) SEM images showing the orientation of the same tube before (main image) and after (right-bottom inset) the pull-out test. (ii) fracture of a tube during the pull-out test: SEM images showing the same tube (c) before and (d) after the tube fracture. (iii) Telescopic pull-out of a tube: SEM images showing the same tube (e) before and (f) after the telescopic pull-out. The inset drawing schematically shows the telescopic pull-out of a DWCNT. All scale bars represent 500 nm. (A colour version of this figure can be viewed online.)

pull-out tests were also experimentally observed: (1) the tube was fractured and its embedded portion remained inside the matrix; (2) a telescopic pull-out of the tube occurred and its embedded portion remained inside the matrix. Fig. 2(c) and (d) shows two selected snapshots of one representative mea-

surement that display the first scenario. In this measurement, the tube was fractured at its protruding segment, while its embedded portion inside the polymer remained intact. It is noted that the fracturing of the tube is caused by the normal stress in the tube, which remains the same in its protruding

segment and starts to decrease with its entry depth into the polymer. Because the normal stress in the tube is always higher at its protruding portion than its embedded segment, the chance of the tube fracture at its embedded portion is quite low, if not impossible. Therefore, the measured embedded length after the tube was pulled out of the polymer as illustrated in Fig. 1(c) represents the actual contact length of the tube inside the polymer. Because DWCNTs were used in our tests, it is possible that the outer tube shell, which was

attached to the AFM force sensor, might be broken first, leading to a telescopic pull-out of the inner tube shell (i.e., the second scenario). The SEM snapshots shown in Fig. 2(e) and (f) display one such telescopic pull-out measurement. The event of the telescopic pull-out can be identified from comparing the lateral sizes of the protruding (i.e., double-walled) and the pulled-out tube segments (i.e., single-walled) of the tested tube shown in the recorded SEM images, as schematically shown in the inset of Fig. 2(f). By comparing the two

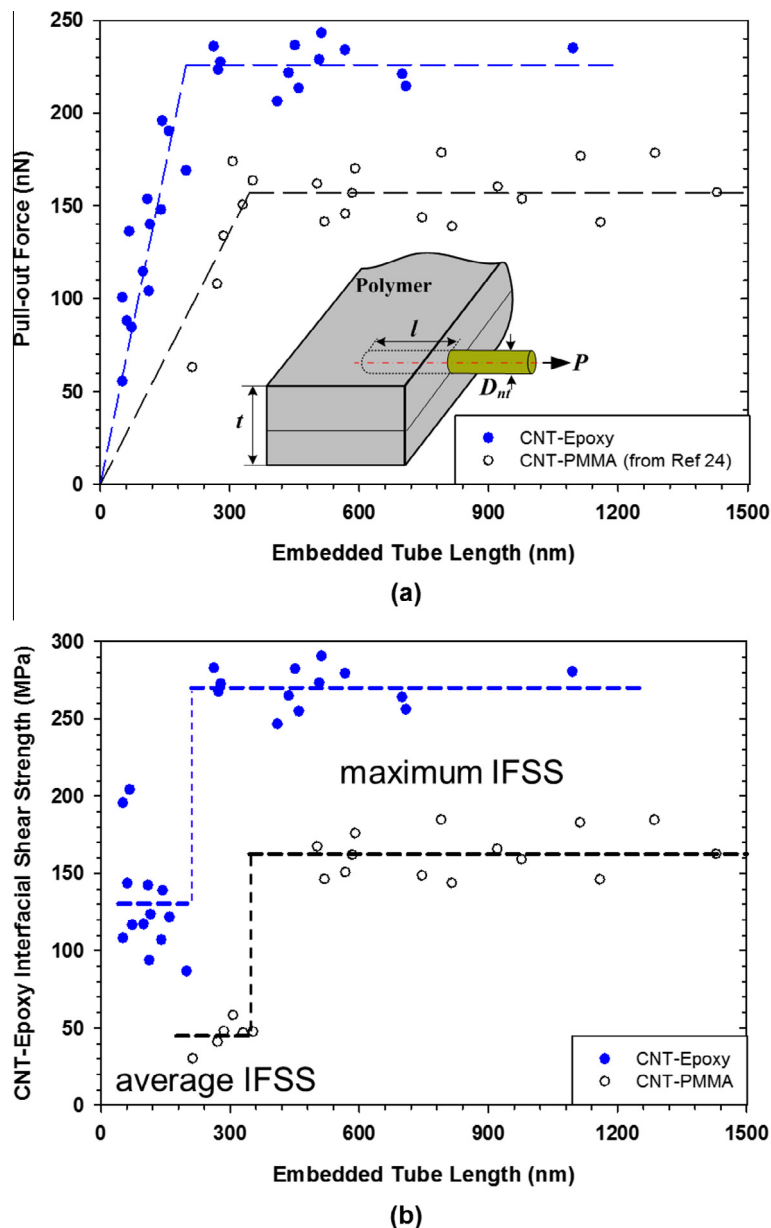


Fig. 3 – (a) The measured dependence of the pull-out load on the embedded tube length. The solid dots represent the data recorded on CNT–epoxy interface. The empty circles represent the recently published data on CNT–PMMA interface that are reproduced from Ref. [24]. The dashed lines represent the respective linear fitting curves to the data set whose tube embedded lengths are below or above the critical embedded length. The inset schematic drawing illustrates the critical parameters in the single-tube pull-out test: P is the pull-out load; l is the nanotube embedded length; D_{nt} is the nanotube outer diameter; and t is the total thickness of the thin film polymer. **(b)** The calculated average and maximum interfacial shear strength (IFSS) of CNT–epoxy interfaces. The vertical dashed lines refer to the locations of the respective critical embedded lengths. (A colour version of this figure can be viewed online.)

snapshots shown in Fig. 2(e) and (f), it can be seen that the outer tube shell broke at the position indicated by the red arrow. Because the contact between the nanotube and the polymer remains intact in the telescopic pull-out, the data recorded in such measurements does not indicate the actual strength of the nanotube–polymer interface.

3.2. Pull-out load versus embedded tube length

We performed a number of single-tube pull-out tests on the DWCNT–epoxy samples using the nanomechanical characterization illustrated in Fig. 1(a)–(c). Among them, 26 measurements were identified to yield successful pull-out of the embedded tube segment as the one shown in Fig. 1(d)–(f). The solid circle curve in Fig. 3(a) shows the dependence of the pull-out load on the embedded tube length recorded in these measurements. The embedded tube length is found to range from 53 nm to 1100 nm, and the measured pull-out load ranges from 55 nN to 243 nN. Our results show that the pull-out load is initially in an increasing trend with the tube embedded length up to 200 nm, and then fluctuates within a band range of 206–243 nN even after a fivefold increase of the embedded length. The observed fluctuation of the pull-out force is attributed to the variations of the nanotube diameter and the nanotube–polymer interface. The observed dependence of the pull-out load on the embedded tube length is a clear indication of the shear lag effect on the failure of the CNT–epoxy interface. The nanotube pull-out process occurs as interfacial debonding through crack propagation. It is noted that the crack on the tube–polymer interface always initiates at the tube entry position. The interface debonding process leads to a saturated pull-out load when the embedded length exceeds a threshold value named as “critical embedded length”. The shear lag effect in the nanotube pull-out process indicates that an effective shear load transfer on the nanotube–polymer interface occurs only within the critical embedded length range. In this work, the critical embedded length for the tested DWCNT–epoxy interface is estimated to be the length value corresponding to the cross point of the two dashed lines shown in Fig. 3(a), and is found to be about 200 nm, which corresponds to a nominal tube aspect ratio of about 65. It is noted that the shear lag effect was also observed on DWCNT–PMMA interfaces that were recently characterized using the same testing techniques and same batch of CNT samples [24]. For the purpose of comparison, the recently reported data on the DWCNT–PMMA interface are also plotted in Fig. 3(a) (empty circles), which shows a critical embedded length of about 350 nm or a nominal tube aspect ratio of 113. It can be clearly seen that the required load for pulling out CNTs from epoxy is consistently higher than from PMMA. The horizontal dashed lines in Fig. 3(a) mark the average values of the pull-out load within the respective bands, which are calculated to be 226 nN for CNT–epoxy interface and 157 nN for CNT–PMMA interfaces. Because the same batch of DWCNT tubes were employed in the studies of these two types of CNT–polymer interfaces, our results reveal that the maximum pull-out load of CNT–epoxy interfaces is, on an average basis, about 44% higher than that of CNT–PMMA interfaces. The critical embedded length for CNT–epoxy interfaces is 43% shorter than that of CNT–PMMA interfaces. The observed

difference in the critical embedded length is mainly ascribed to the different stress distribution and stored elastic energy along the length of the tube–polymer interface, both of which are dependent on the Young’s modulus of the polymer. Because epoxy possesses a much higher modulus than PMMA, the stored elastic energy, which is required to propagate an interfacial crack through the tube–polymer interface region, reaches a saturated value with a shorter embedded length for CNT–epoxy interfaces, compared to that for CNT–PMMA interfaces. To the best of our knowledge, our study is the first reported work on comparing two different types of nanotube–polymer interfaces using the same experimental characterization techniques and the same batch of nanotubes. Our findings on the dependence of the pull-out load on the embedded tube length for different types of polymers are useful in the optimal design of nanotube-reinforced polymer nanocomposites, in particular for the selection of polymer matrices and the geometrical dimensions of nanotubes fillers.

3.3. Interfacial fracture energy and interfacial strength

To compare our data on the strength of CNT–epoxy interfaces with prior results reported in the literature, we calculate the interfacial fracture energy and interfacial shear strength (IFSS) based on our single-tube nanomechanical measurements. The inset drawing in Fig. 3(a) illustrates some of the key physical quantities in our single-tube pull-out scheme that are used in calculating these parameters: the outer diameter of the nanotube D_{nt} ; its initial embedded length l ; the pull-out load P ; and the total thickness of the polymer film t .

Neglecting the friction effect at the interface, the interfacial fracture energy, G_c , is given by [36]

$$G_c = \frac{2}{\pi^2} \frac{(1 + \csc h^2(2n \times l/D_{nt}))}{E_{nt} \times D_{nt}} \left(\frac{P}{D_{nt}} \right)^2, \quad (1)$$

where E_{nt} is the nanotube’s Young’s modulus. n is a parameter given by $n = \sqrt{\frac{E_m}{E_{nt}(1+\nu_m)} \log(t/D_{nt})}$, in which E_m and ν_m are the Young’s modulus and Poisson’s ratio of polymers, respectively. It is noted that both the quantified interfacial fracture energy and the interfacial strength are dependent on the tube diameter employed in the calculation. Because the diameters of the tested tubes (2–4.2 nm) are quite close to the resolution limit of the electron beam and thus could not be measured precisely on the spot, we employ the statistical values of the nanotubes’ diameters measured by AFM in the analysis of the interfacial strength [24]. In the following analysis and discussion, we focus on the results obtained using the median tube diameter (3.1 nm), which are considered to be most representative of the measured CNT–polymer interfacial properties. The data based on the lower and upper limits of the nanotube diameter (i.e., 2.0 nm and 4.2 nm) are also calculated and summarized in Table 1. The following parameters are employed in the calculation: $E_{nt} = 1$ TPa [37]; $E_m = 2.8$ GPa [38]; $t = 2$ μ m; and $\nu_m = 0.33$ [39]. G_c is calculated to be within 0.29–0.40 J/m² based on the median tube diameter. The two solid lines shown in Fig. S2 (see Supplementary Materials) represent the theoretical curves between the pull-out load and the embedded length based on the lower and upper limits of the calculated values of G_c . The full range of G_c (0.116–1.5 J/m²) is consistent with both the data (0.05–0.25 J/m²) reported

by Lou et al. [21] on the interface of MWCNTs with Epon 828 and the data ($1.9 \pm 0.9 \text{ J/m}^2$) reported by Chasiotis et al. [14] for the interface of CNFs with Epon 828. Atomistic simulations were also performed to investigate the nanoscale interfacial fracture toughness between graphene and Epon 828 [40]. The interfacial fracture energy is reported to be about 0.203 J/m^2 , which is also consistent with our data. It is noted that the interfacial adhesion interactions between CNTs and polymers were also characterized by several other techniques, such as sessile-drop, capillary rise and drop-on-fiber methods. Notably, Kim et al. reported the interfacial adhesion energies between pristine multi-walled CNTs and a variety of carbon-based polymers (e.g., Polystyrene (PS) and Polyethylene (PE)) to be within the range of $73\text{--}89 \text{ mJ/m}^2$ [41,42]. The reported values are slightly lower than the data obtained on the CNT–epoxy interface in the present study, but are comparable to the data reported on the CNT–PMMA interface ($54\text{--}800 \text{ mJ/m}^2$) [24].

We evaluate the interfacial shear stress (IFSS) of CNT–epoxy interfaces using two criteria, including the *average IFSS*, by assuming uniform stress on the entire interface and the *maximum IFSS* that occurs at the tube entry position. It is noted that the interfacial shear stress is developed on the tube–polymer interface in response to the applied stretching force on the tube. The value of the shear stress is actually distributed non-uniformly across the entire tube–polymer interface. The shear stress has its maximum value at the tube entry position and decays nearly exponentially with the tube entry depth into the polymer. The average IFSS is calculated based on the whole interfacial area that is given by $\tau_{ave} = \frac{P}{\pi \cdot l \cdot D_{nt}}$, and is only meaningful for a relatively short embedded length, for which the pull-out load is in a nearly linearly proportional relationship with the embedded length. The solid-dot curve on the left side of the vertical line in Fig. 3(b) shows the calculated average IFSS of the CNT–epoxy interface based on the median tube diameter, which is found to be $130 \pm 34 \text{ MPa}$ for $l < 200 \text{ nm}$. Our data on the average IFSS are consistent with the simulation results reported by Liu et al. and Wong et al. [25,26] and the experimental results reported on the CNF–Epon 828 interface [14], while substantially higher than the value reported on MWCNT–Epon 828 interface [21]. Fig. 3(b) also shows that the average IFSS of CNT–epoxy interfaces is substantially higher than that of CNT–PMMA interfaces, which is found to be $45 \pm 9 \text{ MPa}$.

The maximum IFSS, which occurs at the tube entry position, is given as [43,44]

$$\tau_{max} = \frac{2P \cdot n}{\pi \cdot D_{nt}^2 \cdot \tan h(2n \times l/D_{nt})}. \quad (2)$$

The solid-dot curve on the right side of the vertical line in Fig. 3(b) shows the calculated maximum IFSS on the CNT–epoxy interface based on the median tube diameter for the measurements above the critical embedded length in Fig. 3(a). The maximum IFSS is found to be about $270 \pm 12 \text{ MPa}$ for $l > 200 \text{ nm}$. Our result is quite close to the data reported on the CNF–epoxy interface ($224 \pm 60 \text{ MPa}$) [14]. CNFs reportedly have much larger surface roughness than CNTs, which inevitably benefits the shear stress transfer on the fiber–polymer interface through the inter-locking mechanism. The comparable interfacial strength between

CNF/CNT with polymer confirms that CNTs are superior filler materials for polymer nanocomposites. On a comparison basis, the maximum IFSS of CNT–PMMA interfaces is found to be $163 \pm 15 \text{ MPa}$, based on the data (empty dots) shown in Fig. 3(b). Therefore, our results show that the maximum IFSS of CNT–epoxy interfaces is 65.6% higher than that of CNT–PMMA interfaces.

3.4. Molecular dynamics simulation of CNT–polymer interfaces

In this section, we present an analysis of the strengths of the two types of CNT–polymer interfaces that were characterized in the nanomechanical measurements with the aid of molecular dynamics simulations. Our simulations and discussion focus on the molecular deformations of polymer chains that bind to the nanotube surface, and aim to explain the molecular mechanism accounting for the observed difference in the strength of CNT–epoxy and CNT–PMMA interfaces.

Fig. 4(a) and (b) illustrates the chemical structures of epoxy (Epon 828 and curing agent aminoethyl piperazine (AEP)) and PMMA, respectively. In the chemical structure of epoxy, n could be equal to 0, 1 or 2. In the following discussion as well as in the MD simulations, $n = 1$ is employed based on the weight ratio of Epon 828 and curing agent used in the experiment. The chemical compositions and their respective atomic percentage are listed in Table 2. It can be seen that these two types of polymers have quite similar chemical compositions. The percentage of hydrogen (H) atoms in epoxy (51.8%) is slightly lower compared with PMMA (54.1%), while the percentage of carbon (C) atoms is relatively higher in epoxy (39.5%) compared with PMMA (32.8%). Nitrogen (N) atoms account for 2.6% of total atoms in epoxy and come exclusively from the curing agent, but are absent in PMMA. The latter contains higher percentage of oxygen (O) atoms (13.1%) than the former (6.1%). It is noted that N atoms with lone electron pairs in the amine groups reportedly have strong physisorption binding strength with C atoms (in CNTs) due to the strong electrostatic interactions ascribed to polarized electronic structures [45–49]. Therefore, the composition of N atoms in epoxy contributes to the higher binding strength of CNT–epoxy interfaces. However, due to their low atomic percentage, their contribution is considered to be limited, thus not high enough to account for the 44% higher pull-out load observed for epoxy.

Even though both polymers have similar chemical compositions, their molecular structures are quite different from each other. In particular, 21% of C atoms in epoxy exist in the form of four aromatic rings, all of which are located in the polymer backbone. Such aromatic carbon rings are absent in the molecular structures of PMMA chains, in which the C atoms either exist on the polymer backbone in a linear chain form or on the side branches (i.e., the ester groups). Prior studies show that aromatic rings in polymers have a substantial influence on their binding strength with nanotubes [34,48–50]. Both the distance and orientation of the aromatic rings with respect to the nanotube surface matter for their vdW interactions. It is noted from Fig. 4(a) that an aromatic ring is made of three C–C and three C=C bonds, and is tethered to the polymer backbone through one C–O and one C–C

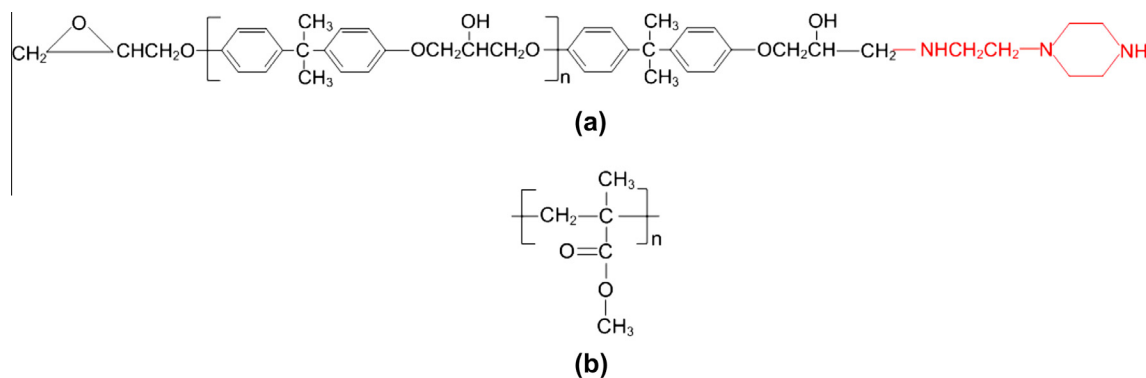


Fig. 4 – (a) Chemical structure of Epon 828 units (in black) crossed linked with one AEP unit (in red). (b) Chemical structure of PMMA units. (A colour version of this figure can be viewed online.)

Table 2 – Chemical compositions of epoxy (Epon 828 crossed linked AEP, assuming $n = 1$ in its molecule structure) and PMMA and their atomic percentages.

Polymer matrix	Percentage of chemical elements				% of C atoms in aromatic rings
	C	H	N	O	
Epoxy	39.5%	51.8%	2.6%	6.1%	21%
PMMA	32.8%	54.1%	–	13.1%	–

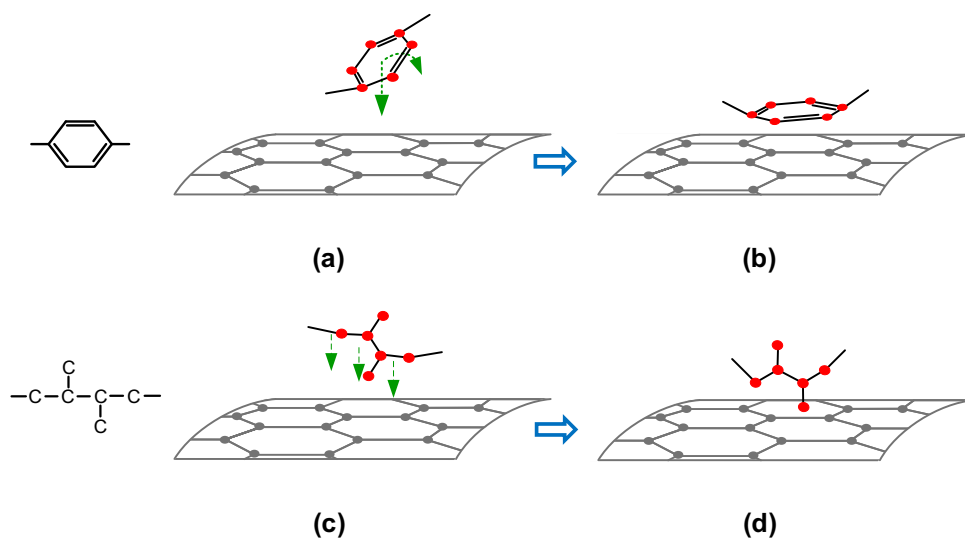


Fig. 5 – The projected molecular conformation transitions in epoxy and PMMA chains due to their respective binding interaction with CNT: (a) and (b) show the original and deformed conformations of an aromatic ring, respectively; (c) and (d) show the original and deformed conformations of a representative polymer backbone that is composed of six carbon atoms, respectively. (A colour version of this figure can be viewed online.)

bonds, which are positioned on the opposite side of the aromatic ring. In addition, each of those C atoms, which are not connected directly to the polymer backbones, also possesses one C–H bond. All the C and H atoms in an aromatic ring stay in the same plane and behave like a rigid structure. The drawings shown in Fig. 5(a) and (b) illustrate how an aromatic ring may move on the surface of a nanotube. The attractive vdW force exerted on all the C atoms in the aromatic ring can be simplified as a concentrated load applied

on the ring center plus a bending moment. The concentrated load will try to bring the aromatic ring closer to the nanotube surface, while the bending moment will induce a rotation of the aromatic ring so that its orientation angle with the CNT binding surface will become smaller. It is noted that the tethering bonds on the two sides of the aromatic ring will be under stretching/compression or rotation to accommodate the displacement of the aromatic ring. In contrast, the vdW forces applied to the C atoms in PMMA are rather distributed

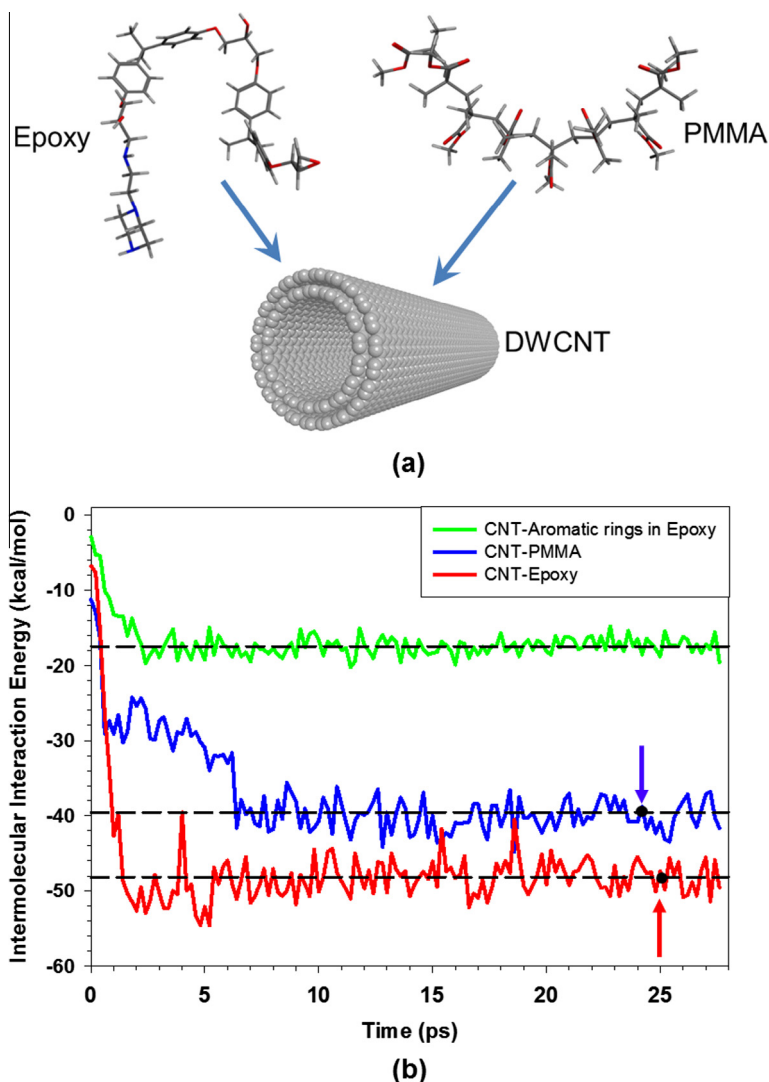


Fig. 6 – (a) Molecular structures of the model epoxy and PMMA chains and the DWCNT employed in the MD simulation. (b) The calculated intermolecular interaction energy between each model polymer chain and the same DWCNT during the relaxation process. The green curve shows the binding energy contributed by the carbon atoms in the aromatic rings in the model epoxy chain. (A colour version of this figure can be viewed online.)

loads with relatively small magnitudes, and their influence on molecular structure of PMMA is somewhat limited, as illustrated in Fig. 5(c) and (d). It is noted that the side ester groups in PMMA structures also hinders the closing of the PMMA backbone to the nanotube surface, and thus has a limiting effect on the interface binding interaction [51].

From an energy point of view, the relaxation of polymer chains on a nanotube surface is mainly driven by the tube-polymer vdW interaction and steric hindrance [52,53]. On one hand, energy is released through the work done by the attractive vdW force, and the total intermolecular energy or vdW energy, which carries a negative sign, decreases. On the other hand, the work done by the vdW force affects the molecular conformation of the polymer, which is accompanied by bond deformation (i.e., stretching or compression) and/or rotation. The bond rotation in polymer chains leads to the twisting of polymer backbones and energy dissipation.

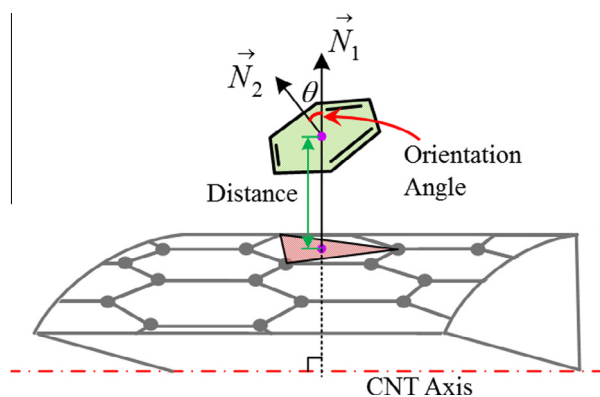


Fig. 7 – Schematic of an aromatic ring on the surface of a nanotube. (A colour version of this figure can be viewed online.)

Therefore, the physisorption binding of a polymer on a nanotube surface will result in changes of the elasticity energy stored in the polymer. Below, we investigate the relaxation of epoxy and PMMA chains on the surface of nanotubes using MD simulations.

The molecular structures shown in Fig. 6(a) illustrate the model CNT and the model polymer chains employed in the MD simulations: (1) a DWCNT that has an outer diameter of 3.1 nm (i.e., the median diameter of the tested tubes) and a length of 10 nm; (2) a PMMA chain that is composed of eight monomer units (122 atoms in total); (3) an epoxy chain that is composed of two units of Epon 828 (i.e., $n = 1$ in the chemical structure shown in Fig. 4(a)) and one unit of curing agent EAP (114 atoms in total). The model molecules are better described as oligomers than polymers; however, we use the term “polymer” in this section for consistency. The model PMMA and epoxy chains are initially placed along the side of the DWCNT within the cutoff distance. Subsequently, they are adsorbed onto the DWCNT surface due to the attractive

vdW force. For both the PMMA and the epoxy chains, different initial conditions are studied to ensure that the calculated adsorption energy does not depend on their initial conformations. If the simulation time were long enough, all the states of the interface could be explored. The blue and red curves in Fig. 6(b) show the evolution of the intermolecular interaction energy during the relaxation of the respective polymer chains on the surface of the same nanotube. It can be clearly seen that the interaction energy for both polymers has an initial decreasing trend with the relaxation time and then tends to reach a steady state asymptotically. The magnitude of the steady-state intermolecular interaction energy provides a direct measure of the strength of the binding energy between the polymer chains and the DWCNT. It can be seen that the epoxy chain possesses a stronger binding interaction (-48.1 kcal/mol) with the DWCNT compared with the PMMA chain (-39.6 kcal/mol). Considering the fact that the employed model epoxy chain has 7% fewer atoms than the model PMMA chain, the interfacial energy between the model

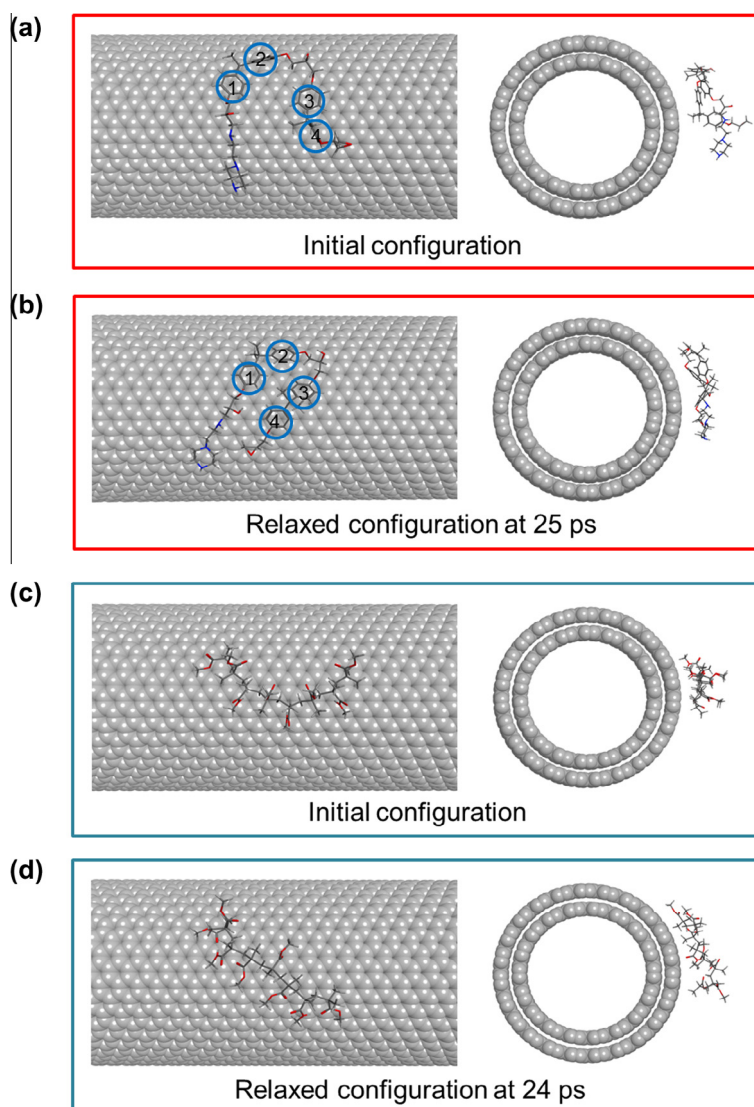


Fig. 8 – Selected MD snapshots showing the original and relaxed conformations of the modeled epoxy (a and b) and PMMA (c and d) chains on the surface of the same model DWCNT. (A colour version of this figure can be viewed online.)

Table 3 – Comparison of the orientation angle and distance of each aromatic ring in the model epoxy chain with respect to the model CNT surface between their initial and relaxed states.

Index of aromatic rings	Orientation Angle θ ($^\circ$)		Distance (\AA)	
	Initial	Relaxed	Initial	Relaxed
Ring 1	32.14	34.92	7.16	4.41
Ring 2	72.16	26.19	7.33	4.20
Ring 3	25.33	38.65	5.54	4.48
Ring 4	88.01	18.06	7.59	4.06

epoxy chain and the CNT is found, on a per atom basis, to be 30% higher than that of CNT–PMMA interfaces.

The green curve in Fig. 6(b) shows the interaction energy contributed only by the C atoms in the aromatic rings in epoxy. The results show that the average steady-state binding energy (-17.5 kcal/mol) between the C atoms of the four aromatic rings in epoxy and the DWCNT makes a valuable contribution to the whole binding energy: 21% of the aromatic atoms contribute to 36.4% of the total binding energy. Our results are consistent with the prior findings that aromatic rings on the polymer backbone are able to align parallel to the nanotube surface and form strong π – π interaction on the tube–polymer interface [34,50,51,54,55]. Our MD results show that the substantial binding energy contributed by the aromatic rings results from their orientation angle and distance changes with respect to the nanotube surface. Fig. 7 schematically shows an aromatic ring on the surface of a nanotube. Here, the orientation angle θ is defined as the acute angle formed by the normal axis of the ring plane with the projection vector of the ring center on the nanotube central axis. The distance is defined as the difference of the distance of the ring center to the nanotube central axis and the outer radius of the nanotube.

The selected MD snapshots in Fig. 8 show the initial and the steady-state conformations of the model polymer chains on the surface of the nanotube. For both polymers, the selected steady-state conformations correspond to the respective average steady-state binding energy, as indicated by the arrows shown in Fig. 6(b). It can be seen that the epoxy chain orientates its aromatic ring planes to align with, and also moves closer to, the surface of the DWCNT to achieve a low potential energy status. The prominent binding interaction between the aromatic rings in the model epoxy and the DWCNT breaks the initial energy-minimized configuration of the epoxy chain and generates local net forces to trigger the alignment motion of the rest of the epoxy chain to the surface of the DWCNT. This process repeats until a new equilibrium state is reached. There are four aromatic rings in the model epoxy chain as marked by the circles in Fig. 8(a). We check the change of the orientation angle and the distance of each aromatic ring with respect to the nanotube surface during the relaxation process, and the results are listed in Table 3. The initial distances of the aromatic rings to the nanotube surface are found to be within 5.54–7.59 \AA , which are contrasted with the much smaller values of 4.06–4.48 \AA for the steady-state shown in Fig. 8(b). On average, the distance of the aromatic ring to the surface of the nanotube decreases by 37%. Therefore, it is quite clear that the all the

aromatic rings move closer to the nanotube surface during the relaxation process. Unlike the clear trend shown in the ring distance, the results for the ring's orientation angle show two opposite changes. As listed in Table 3, the results show a substantial decrease of the orientation angle for rings 2 and 4, while there is a modest increase for rings 1 and 3. On an average basis, the orientation angle of each aromatic ring decreases by about 25° . The orientation change of the aromatic ring to be parallel to the nanotube surface facilitates the formation of strong π – π interaction on the tube–polymer interface, which contributes to the increase of the binding energy. For the model PMMA chain, the snapshots shown in Fig. 8(c) and (d) show that it rotates on the DWCNT surface and does not have an obvious aligning process except for a slight wrapping process, which is also an important phenomenon for the CNT–polymer interaction [34]. The steady-state of the polymer chain on the surface of the tube is also a kinetic process, which can be clearly seen from the fluctuation in all the binding energy curves shown in Fig. 6(b). However, the quite small magnitude of the fluctuation suggests that the variation of the distance and orientation angle of all the aromatic rings are also in relatively small ranges. Therefore, even though the steady-state results shown in Fig. 8 are time-dependent, the analysis based on these results is still valid.

4. Conclusion

In summary, we present a quantitative experimental study of the CNT–epoxy interfacial strength using *in situ* electron microscopy nanomechanical single-tube pull-out techniques. Our results, for the first time, reveal that the maximum pull-out load of CNT–epoxy interfaces is 44% stronger than that of CNT–PMMA interfaces. Our MD simulations show that substantial molecular conformation changes in epoxy chains occur in reaction to their vdW interaction with the nanotube surface, which, in turn, result in a strong binding interface. This study demonstrates that our *in situ* nanomechanical single-tube experimental technique can be used to characterize the unique nanomechanical signatures of the interfaces formed by CNTs with a variety of polymer matrices, thus enabling a convincing quantification and comparison of the interfacial strength across different nanotube–polymer material systems. The research findings presented in this paper contribute to a better understanding of the load transfer on the tube–polymer interface and the tube's reinforcing mechanism, and ultimately the optimal design and performance of nanotube-reinforced polymer nanocomposites.

Acknowledgements

This work was funded by US Air Force Office of Scientific Research. The single-tube nanomechanical pull-out measurements were performed using the facilities in the Analytical and Diagnostics Laboratory at Binghamton University's Small Scale Systems Integration and Packaging Center (S3IP). The facility support for molecular dynamics simulations from the Georgia Advanced Computing Resource Center at University of Georgia was greatly appreciated.

Appendix A. Supplementary data

Supplementary data associated with this article can be found, in the online version, at <http://dx.doi.org/10.1016/j.carbon.2014.10.065>.

REFERENCES

- [1] Moniruzzaman M, Winey KI. Polymer nanocomposites containing carbon nanotubes. *Macromolecules* 2006;39:5194–205. <http://dx.doi.org/10.1021/ma060733p>.
- [2] Cheng Q, Wang B, Zhang C, Liang Z. Functionalized carbon-nanotube sheet/bismaleimide nanocomposites: mechanical and electrical performance beyond carbon-fiber composites. *Small* 2010;6:763–7. <http://dx.doi.org/10.1002/sml.200901957>.
- [3] Iijima S. Helical microtubules of graphitic carbon. *Nature* 1991;354:56–8.
- [4] Jia Z, Wang Z, Xu C, Liang J, Wei B, Wu D, et al. Study on poly(methyl methacrylate)/carbon nanotube composites. *Mater Sci Eng: A* 1999;271:395–400. [http://dx.doi.org/10.1016/S0921-5093\(99\)00263-4](http://dx.doi.org/10.1016/S0921-5093(99)00263-4).
- [5] Haggemueller R, Du F, Fischer JE, Winey KI. Interfacial in situ polymerization of single wall carbon nanotube/nylon 6,6 nanocomposites. *Polymer* 2006;47:2381–8. <http://dx.doi.org/10.1016/j.polymer.2006.01.087>.
- [6] Leelapornpisit W, Ton-That M-T, Perrin-Sarazin F, Cole KC, Denault J, Simard B. Effect of carbon nanotubes on the crystallization and properties of polypropylene. *J Polym Sci, Part B: Polym Phys* 2005;43:2445–53. <http://dx.doi.org/10.1002/polb.20527>.
- [7] Minus ML, Chae HG, Kumar S. Single wall carbon nanotube templated oriented crystallization of poly(vinyl alcohol). *Polymer* 2006;47:3705–10. <http://dx.doi.org/10.1016/j.polymer.2006.03.076>.
- [8] Chae HG, Minus ML, Kumar S. Oriented and exfoliated single wall carbon nanotubes in polyacrylonitrile. *Polymer* 2006;47:3494–504. <http://dx.doi.org/10.1016/j.polymer.2006.03.050>.
- [9] Ding W, Eitan A, Fisher FT, Chen X, Dikin DA, Andrews R, et al. Direct observation of polymer sheathing in carbon nanotube–polycarbonate composites. *Nano Lett* 2003;3:1593–7. <http://dx.doi.org/10.1021/nl0345973>.
- [10] Zhang Y, Song K, Meng J, Minus ML. Tailoring polyacrylonitrile interfacial morphological structure by crystallization in the presence of single-wall carbon nanotubes. *ACS Appl Mater Interfaces* 2013;5:807–14. <http://dx.doi.org/10.1021/am302382m>.
- [11] Liu Y, Kumar S. Polymer/carbon nanotube nano composite fibers – a review. *ACS Appl Mater Interfaces* 2014;6:6069–87. <http://dx.doi.org/10.1021/am405136s>.
- [12] Newcomb BA, Chae HG, Gulgunje PV, Gupta K, Liu Y, Tsentelovich DE, et al. Stress transfer in polyacrylonitrile/carbon nanotube composite fibers. *Polymer* 2014;55:2734–43. <http://dx.doi.org/10.1016/j.polymer.2014.04.008>.
- [13] Roy D, Bhattacharyya S, Rachamim A, Plati A, Saboungi M-L. Measurement of interfacial shear strength in single wall carbon nanotubes reinforced composite using Raman spectroscopy. *J Appl Phys* 2010;107. <http://dx.doi.org/10.1063/1.3295907>. 043501-043501-6.
- [14] Ozkan T, Chen Q, Chasiotis I. Interfacial strength and fracture energy of individual carbon nanofibers in epoxy matrix as a function of surface conditions. *Compos Sci Technol* 2012;72:965–75. <http://dx.doi.org/10.1016/j.compscitech.2012.03.004>.
- [15] Manoharan MP, Sharma A, Desai AV, Haque MA, Bakis CE, Wang KW. The interfacial strength of carbon nanofiber epoxy composite using single fiber pullout experiments. *Nanotechnology* 2009;20:295701. <http://dx.doi.org/10.1088/0957-4484/20/29/295701>.
- [16] Tsuda T, Ogasawara T, Deng F, Takeda N. Direct measurements of interfacial shear strength of multi-walled carbon nanotube/PEEK composite using a nano-pullout method. *Compos Sci Technol* 2011;71:1295–300. <http://dx.doi.org/10.1016/j.compscitech.2011.04.014>.
- [17] Cooper CA, Cohen SR, Barber AH, Wagner HD. Detachment of nanotubes from a polymer matrix. *Appl Phys Lett* 2002;81:3873–5. <http://dx.doi.org/10.1063/1.1521585>.
- [18] Barber AH, Cohen SR, Wagner HD. Measurement of carbon nanotube–polymer interfacial strength. *Appl Phys Lett* 2003;82:4140. <http://dx.doi.org/10.1063/1.1579568>.
- [19] Barber AH, Cohen SR, Kenig S, Wagner HD. Interfacial fracture energy measurements for multi-walled carbon nanotubes pulled from a polymer matrix. *Compos Sci Technol* 2004;64:2283–9. <http://dx.doi.org/10.1016/j.compscitech.2004.01.023>.
- [20] Barber AH, Cohen SR, Eitan A, Schadler LS, Wagner HD. Fracture transitions at a carbon-nanotube/polymer interface. *Adv Mater* 2006;18:83–7. <http://dx.doi.org/10.1002/adma.200501033>.
- [21] Ganesan Y, Peng C, Lu Y, Loya PE, Moloney P, Barrera E, et al. Interface toughness of carbon nanotube reinforced epoxy composites. *ACS Appl Mater Interfaces* 2011;3:129–34. <http://dx.doi.org/10.1021/am1011047>.
- [22] Ganesan Y, Salahshoor H, Peng C, Khabashesku V, Zhang J, Cate A, et al. Fracture toughness of the sidewall fluorinated carbon nanotube–epoxy interface. *J Appl Phys* 2014;115:224305. <http://dx.doi.org/10.1063/1.4881882>.
- [23] Wagner HD, Lourie O, Feldman Y, Tenne R. Stress-induced fragmentation of multiwall carbon nanotubes in a polymer matrix. *Appl Phys Lett* 1998;72:188–90. <http://dx.doi.org/10.1063/1.120680>.
- [24] Chen X, Zheng M, Park C, Ke C. Direct measurements of the mechanical strength of carbon nanotube–poly(methyl methacrylate) interfaces. *Small* 2013;9:3345–51. <http://dx.doi.org/10.1002/sml.201202771>.
- [25] Liu JQ, Xiao T, Liao K, Wu P. Interfacial design of carbon nanotube polymer composites: a hybrid system of noncovalent and covalent functionalizations. *Nanotechnology* 2007;18:165701. <http://dx.doi.org/10.1088/0957-4484/18/16/165701>.
- [26] Wong M, Paramsothy M, Xu XJ, Ren Y, Li S, Liao K. Physical interactions at carbon nanotube–polymer interface. *Polymer* 2003;44:7757–64. <http://dx.doi.org/10.1016/j.polymer.2003.10.011>.
- [27] Gou J, Minaie B, Wang B, Liang Z, Zhang C. Computational and experimental study of interfacial bonding of single-walled nanotube reinforced composites. *Comput Mater Sci*

- 2004;31:225–36. <http://dx.doi.org/10.1016/j.commat.2004.03.002>.
- [28] Cui S, Canet R, Derre A, Couzi M, Delhaes P. Characterization of multiwall carbon nanotubes and influence of surfactant in the nanocomposite processing. *Carbon* 2003;41:797–809. [http://dx.doi.org/10.1016/S0008-6223\(02\)00405-0](http://dx.doi.org/10.1016/S0008-6223(02)00405-0).
- [29] Gong X, Liu J, Baskaran S, Voise RD, Young JS. Surfactant-assisted processing of carbon nanotube/polymer composites. *Chem Mater* 2000;12:1049–52. <http://dx.doi.org/10.1021/cm9906396>.
- [30] Jorgensen WL, Maxwell DS, Tirado-Rives J. Development and testing of the OPLS all-atom force field on conformational energetics and properties of organic liquids. *J Am Chem Soc* 1996;118:11225–36. <http://dx.doi.org/10.1021/ja9621760>.
- [31] Berendsen HJC, Postma JPM, van Gunsteren WF, DiNola A, Haak JR. Molecular dynamics with coupling to an external bath. *J Chem Phys* 1984;81:3684–90. <http://dx.doi.org/10.1063/1.448118>.
- [32] Ke CH, Pugno N, Peng B, Espinosa HD. Experiments and modeling of carbon nanotube-based NEMS devices. *J Mech Phys Solids* 2005;53:1314–33.
- [33] Wnuk JD, Rosenberg SG, Gorham JM, van Dorp WF, Hagen CW, Fairbrother DH. Electron beam deposition for nanofabrication: insights from surface science. *Surf Sci* 2011;605:257–66. <http://dx.doi.org/10.1016/j.susc.2010.10.035>.
- [34] Yang M, Koutsos V, Zaiser M. Interactions between polymers and carbon nanotubes: a molecular dynamics study. *J Phys Chem B* 2005;109:10009–14. <http://dx.doi.org/10.1021/jp0442403>.
- [35] Duchamp M, Meunier R, Smajda R, Mionic M, Magrez A, Seo JW, et al. Reinforcing multiwall carbon nanotubes by electron beam irradiation. *J Appl Phys* 2010;108:084314. <http://dx.doi.org/10.1063/1.3493049>.
- [36] Jiang KR, Penn LS. Improved analysis and experimental evaluation of the single filament pull-out test. *Compos Sci Technol* 1992;45:89–103. [http://dx.doi.org/10.1016/0266-3538\(92\)90031-W](http://dx.doi.org/10.1016/0266-3538(92)90031-W).
- [37] Wong EW, Sheehan PE, Lieber CM. Nanobeam mechanics: elasticity, strength, and toughness of nanorods and nanotubes. *Science* 1997;277:1971–5. <http://dx.doi.org/10.1126/science.277.5334.1971>.
- [38] Epon resin structural reference manual. Resolution performance products LLC; 2001.
- [39] May C. *Epoxy resins: chemistry and technology*. second ed. Marcel Dekker; 1988.
- [40] Salahshoor H, Rahbar N. Nano-scale fracture toughness and behavior of graphene/epoxy interface. *J Appl Phys* 2012;112:023510. <http://dx.doi.org/10.1063/1.4737776>.
- [41] Roh SC, Choi EY, Choi YS, Kim CK. Characterization of the surface energies of functionalized multi-walled carbon nanotubes and their interfacial adhesion energies with various polymers. *Polymer* 2014;55:1527–36. <http://dx.doi.org/10.1016/j.polymer.2014.02.015>.
- [42] Choi EY, Roh SC, Kim CK. Noncovalent functionalization of multi-walled carbon nanotubes with pyrene-linked nylon66 for high performance nylon66/multi-walled carbon nanotube composites. *Carbon* 2014;72:160–8. <http://dx.doi.org/10.1016/j.carbon.2014.01.068>.
- [43] Chua PS, Piggott MR. The glass fibre—polymer interface: I—theoretical consideration for single fibre pull-out tests. *Compos Sci Technol* 1985;22:33–42. [http://dx.doi.org/10.1016/0266-3538\(85\)90089-2](http://dx.doi.org/10.1016/0266-3538(85)90089-2).
- [44] Cox HL. The elasticity and strength of paper and other fibrous materials. *Br J Appl Phys* 1952;3:72–9. <http://dx.doi.org/10.1088/0508-3443/3/3/302>.
- [45] Friddle RW, Lemieux MC, Cicero G, Artyukhin AB, Tsukruk VV, Grossman JC, et al. Single functional group interactions with individual carbon nanotubes. *Nat Nano* 2007;2:692–7. <http://dx.doi.org/10.1038/nnano.2007.334>.
- [46] Thong YX, Poon YF, Chen T-Y, Li L-J, Chan-Park MB. Direct intermolecular force measurements between functional groups and individual metallic or semiconducting single-walled carbon nanotubes. *Small* 2014;10:750–7. <http://dx.doi.org/10.1002/smll.201302084>.
- [47] Opatkiewicz JP, Lemieux MC, Bao Z. Influence of electrostatic interactions on spin-assembled single-walled carbon nanotube networks on amine-functionalized surfaces. *ACS Nano* 2010;4:1167–77. <http://dx.doi.org/10.1021/nn901388v>.
- [48] Park C, Wise KE, Kang JH, Kim J-W, Sauti G, Lowther SE, et al. Multifunctional nanotube polymer nanocomposites for aerospace applications: adhesion between SWCNT and polymer matrix. Austin, TX, United States; 2008.
- [49] Wise KE, Park C, Siochi EJ, Harrison JS. Stable dispersion of single wall carbon nanotubes in polyimide: the role of noncovalent interactions. *Chem Phys Lett* 2004;391:207–11. <http://dx.doi.org/10.1016/j.cplett.2004.04.096>.
- [50] Zheng Q, Xue Q, Yan K, Hao L, Li Q, Gao X. Investigation of molecular interactions between SWNT and polyethylene/polypropylene/polystyrene/polyaniline molecules. *J Phys Chem C* 2007;111:4628–35. <http://dx.doi.org/10.1021/jp066077c>.
- [51] Tallury SS, Pasquinelli MA. Molecular dynamics simulations of flexible polymer chains wrapping single-walled carbon nanotubes. *J Phys Chem B* 2010;114:4122–9. <http://dx.doi.org/10.1021/jp908001d>.
- [52] Yang H, Chen Y, Liu Y, Cai WS, Li ZS. Molecular dynamics simulation of polyethylene on single wall carbon nanotube. *J Chem Phys* 2007;127:094902. <http://dx.doi.org/10.1063/1.2768060>.
- [53] Zhang X, Li Z, Yang H, Sun C-C. Molecular dynamics simulations on crystallization of polyethylene copolymer with precisely controlled branching. *Macromolecules* 2004;37:7393–400. <http://dx.doi.org/10.1021/ma030010v>.
- [54] Foroutan M, Nasrabadi AT. Investigation of the interfacial binding between single-walled carbon nanotubes and heterocyclic conjugated polymers. *J Phys Chem B* 2010;114:5320–6. <http://dx.doi.org/10.1021/jp100960u>.
- [55] Liu W, Yang C-L, Zhu Y-T, Wang M. Interactions between single-walled carbon nanotubes and polyethylene/polypropylene/polystyrene/poly(phenylacetylene)/poly(p-phenylenevinylene) considering repeat unit arrangements and conformations: a molecular dynamics simulation study. *J Phys Chem C* 2008;112:1803–11. <http://dx.doi.org/10.1021/jp076561v>.